

Active Brownian particles in power-law viscoelastic media

D. S. Quevedo¹, M. Conte², M. Dijkstra², and C. Morais Smith¹

¹*Institute for Theoretical Physics, Utrecht University,
Princetonplein 5, 3584CC Utrecht, The Netherlands*

²*Soft Condensed Matter and Biophysics, Debye Institute for
Nanomaterials Science, Utrecht University, Utrecht, The Netherlands*

(Dated: December 24, 2025)

Many active particles are embedded in environments that exhibit viscoelastic properties. An important class of such media lacks a single characteristic relaxation timescale when subjected to a time-dependent stress. Rather, the stress response spans a broad continuum of timescales, a behavior naturally described by a scale-free, fractal-like power-law relaxation modulus. Using a generalization of the fractional Langevin equation, we investigate an active Brownian particle embedded in a power-law viscoelastic environment with translational and rotational dynamics governed by independent fractional orders. We solve the model analytically, develop a numerical scheme to validate the theoretical predictions, and provide tools that can be used in further studies. A rich variety of diffusion regimes emerges, which modify the intermediate-time behavior of the mean squared displacement. Notably, we find that the competition between translational and rotational contributions favors a superdiffusive persistence over the standard ballistic motion, and over-stretches its characteristic timescale, fundamentally altering the standard relation between persistence and propulsion in active matter.

Active Brownian particles are an important example of active matter, capable of converting internal energy into directed motion [1–3]. Active-matter systems were originally studied in the context of collective motion at both macroscopic and microscopic scales [4–6]. They subsequently became a central focus because of their ability to describe phenomena across vastly different length scales, from herds of large mammals to bacteria colonies, under minimal modeling assumptions [7, 8]. Particular attention has been given to both biological and synthetic micro-swimmers, micron-sized particles that propel themselves through fluid environments, because of their relevance for the description of bacterial behavior and for the development of engineered self-propelled devices [9, 10]. The interplay between persistent active motion, thermal fluctuations, and environmental interactions, gives rise to a rich variety of emergent phenomena such as anomalous diffusion, clustering, and non-equilibrium phase transitions [11–14].

Often, micro-swimmers are embedded in materials that deviate from the ideal behaviors described by Hooke’s law for elastic solids and Newton’s law for viscous fluids. Instead, such materials exhibit both elastic and viscous responses simultaneously and are therefore classified as viscoelastic [15]. A useful way to characterize their viscoelastic properties is through a relaxation test, which measures the stress response to a time-dependent applied strain. This response is described by the so-called relaxation modulus, which is constant for ideal elastic solids and proportional to a Dirac delta function for purely viscous fluids. The motion of a particle embedded in such a medium can then be modeled using a generalized Langevin equation (GLE), where the memory kernel is related to the relaxation modulus via the generalized Stokes–Einstein relation (GSE) [16, 17].

The form of the memory kernel plays a crucial role in

determining the system’s dynamical behavior. To date, GLEs with exponential memory kernels have been widely employed [18, 19], but a broad class of soft and biological materials exhibits a power-law relaxation modulus that decays as $\chi(t) \propto t^{-\gamma}$ [20]. Using the GSE, the corresponding friction kernel scales as $K(t) \propto t^{-\alpha}$, with $\gamma = \alpha + 1$ [21]. Such power-law responses are characteristic of complex materials possessing a wide distribution of microstructural length and time scales. Important examples include biological tissues [22], gels [23–25], intra- and extracellular components [26–29], polymer networks [30–32], and soft crowded suspensions [17, 33, 34]. Although understanding active motion in these environments is of considerable importance, it remains largely unexplored, with only a few exceptions [35, 36], all of which have been restricted to one-dimensional systems.

Fractional calculus provides a natural framework for describing power-law relaxation moduli and memory kernels. Fractional operators encode scale-free, fractal-like memory, and therefore do not require the introduction of a characteristic timescale. Indeed, fractional models have proven highly successful in describing the rheological behavior of soft biological tissues exhibiting power-law scaling [37–40]. Furthermore, they constitute the cornerstone for the study of anomalous diffusion behavior [41], where the mean squared displacement (MSD) deviates from linear growth and instead scales as t^α . The fractional generalization of the Langevin equation, first introduced by Lutz [42], is particularly relevant in this context. It captures the dynamics of a particle subjected to a dissipative force of non-integer order and to long-range, time-correlated noise. The interplay between dissipation and noise gives rise to slow relaxation dynamics, leading to anomalous diffusion and, more recently, to the emergence of pre-thermal periodic time-ordered phases [43, 44].

In this work, we extend the fractional Langevin equation to model the motion of active Brownian particles, in which both translational and rotational degrees of freedom are influenced by the power-law viscoelastic properties of the surrounding medium. We solve the model analytically and develop numerical expressions suitable for further investigations. The interplay between the fractional orders and the noise acting on the spatial degrees of freedom gives rise to a rich spectrum of anomalous diffusion regimes that modifies the intermediate-time behavior of the MSD favoring superdiffusion over the standard t^2 during the persistence phase and preserving the long-time enhanced normal diffusion that characterizes active particles.

Fractional active Langevin equation—We study the dynamics of an active Brownian particle embedded in a two-dimensional viscoelastic medium, described by its position vector $\mathbf{r}(t) = (x(t), y(t))$ and orientation angle $\phi(t)$. Both state variables evolve according to the following set of overdamped generalized Langevin equations,

$$\begin{aligned} \int_0^t K_T(t-\tau)[\dot{\mathbf{r}}(\tau) - v\hat{\mathbf{n}}(\tau)]d\tau &= \theta_T \xi_T(t), \\ \int_0^t K_R(t-\tau)\dot{\phi}(\tau)d\tau &= \theta_R \xi_R(t), \end{aligned} \quad (1)$$

where $\hat{\mathbf{n}} = (\cos \phi, \sin \phi)$ denotes the direction of self-propulsion with magnitude v , and $\xi_T = (\xi_x, \xi_y)$ and ξ_R are the translational and rotational stochastic forces, respectively, with strengths $\theta_{\{T,R\}}$. The time-delayed viscoelastic response of the medium is captured by a power-law memory kernel,

$$K_Q(t-t') = \frac{\eta_Q(t-t')^{-\alpha_Q}}{\Gamma(1-\alpha_Q)}, \quad (2)$$

where $\alpha_Q \in (0, 1)$, η_Q is the corresponding viscous coefficient, and the subscript $Q = \{T, R\}$ denotes either the translational or rotational component. This choice corresponds to a power-law relaxation modulus of the form $\chi(t) \propto t^{-\alpha_Q}$, characteristic of scale-free viscoelastic media. Using the Caputo fractional derivative [45],

$${}_0^C D_t^{\alpha_Q} \mathbf{f} = \int_{t_0}^t \frac{(t-\tau)^{-\alpha_Q}}{\Gamma(1-\alpha_Q)} \frac{d\mathbf{f}}{d\tau} d\tau, \quad (3)$$

Eqs. (1) can be rewritten as a set of overdamped fractional Langevin equations,

$$\begin{aligned} \eta_T {}_0^C D_t^{\alpha_T} [\mathbf{r}(t) - v\hat{\mathbf{N}}(t)] &= \theta_T \xi_T(t), \\ \eta_R {}_0^C D_t^{\alpha_R} \phi(t) &= \theta_R \xi_R(t), \end{aligned} \quad (4)$$

where the time derivative of $\hat{\mathbf{N}}$ defines the direction of self-propulsion $\hat{\mathbf{n}} = d\hat{\mathbf{N}}/dt$. In the limit $\alpha_Q \rightarrow 1$, the Caputo fractional derivative in Eq. (3) reduces to an ordinary first-order time derivative, and Eqs. (4) recover the conventional overdamped active Langevin dynamics.

In particular, we model the stochastic forces as fractional Gaussian noises with zero mean, $\langle \xi_T(t) \rangle = 0$ and $\langle \xi_R(t) \rangle = 0$, and power-law correlations for $t \neq t'$,

$$\begin{aligned} \mathbb{C}_T &\equiv \theta_T^2 \langle \xi_T(t) \otimes \xi_T(t') \rangle = \mathbb{I} \theta_T^2 H_T (2H_T - 1) |t - t'|^{2H_T - 2}, \\ C_R &\equiv \theta_R^2 \langle \xi_R(t) \xi_R(t') \rangle = \theta_R^2 H_R (2H_R - 1) |t - t'|^{2H_R - 2}, \end{aligned} \quad (5)$$

where \mathbb{I} denotes the 2×2 identity matrix. Isotropy of the medium implies a single, constant Hurst exponent H_T for both translational degrees of freedom, while the rotational noise is characterised by a (generally distinct from the translational one) Hurst exponent H_R .

For simplicity, we assume that the memory kernels are related to the correlation functions of the noise through the fluctuation-dissipation relations of the second kind,

$$\begin{aligned} \mathbb{C}_T(|t - t'|) &= k_B T \mathbb{I} K_T(t - t'), \\ C_R(|t - t'|) &= k_B T K_R(t - t'), \end{aligned} \quad (6)$$

where k_B is the Boltzmann's constant and T the temperature. As a consequence, the order of the fractional derivative and the Hurst exponent are related by $\alpha_Q = 2 - 2H_Q$, and the noise amplitude is given by $\theta_Q^2 = \eta_Q k_B T / [\Gamma(1 - \alpha_Q) H_Q (2H_Q - 1)]$.

The solutions of Eqs. (4) can be obtained using Laplace transform techniques (see Refs. [46, 47]). By Laplace transforming Eqs. (4) and inverting back, we obtain

$$\begin{aligned} \mathbf{r}(t) &= \mathbf{r}_0 + \theta_T (\xi_T * G_T)(t) - v \int_0^t \hat{\mathbf{n}}(\tau) d\tau, \\ \phi(t) &= \phi_0 + \theta_R (\xi_R * G_R)(t), \end{aligned} \quad (7)$$

where $\mathbf{r}_0 = \mathbf{r}(t=0)$, $\phi_0 = \phi(t=0)$, $*$ is the convolution operator, and $G_Q(t)$ is the resolvent function defined as the inverse Laplace transform of $\tilde{G}_Q(s) = 1/[s\tilde{K}_Q(s)]$. Recalling the power-law memory kernel in Eq. (2), whose Laplace transform is $\tilde{K}_Q(s) = \eta_Q s^{\alpha_Q - 1}$, the resolvent function becomes

$$G_Q(t) = \mathcal{L}^{-1}\{\tilde{G}_Q(s); t\} = \frac{t^{\alpha_Q - 1}}{\eta_Q \Gamma(\alpha_Q)}. \quad (8)$$

Numerical solutions of the fractional active Langevin equation—The particle's inertia combined with the slow relaxation dynamics typical of the fractional Langevin equations can give rise to transient pre-thermal effects for small values of α_Q , manifested as periodic oscillations in the velocity autocorrelation and the MSD [43]. This feature poses challenges for simulating fractional overdamped dynamics because numerical algorithms developed for underdamped cases [43, 48] converge slowly to the overdamped limit. To overcome this problem, we use the L1 discretization scheme of the Caputo operator [49] (see App. A of the End Matter), allowing us to tailor the recursive discretized expression for the overdamped rotational and the active translational equations,

$$\begin{aligned} \phi(t_n) &= \phi(t_{n-1}) - \sum_{j=1}^{n-1} c_{n-j} [\phi(t_j) - \phi(t_{j-1})] \\ &+ \frac{\Gamma(2 - \alpha_R)}{h^{-\alpha_R}} \theta_R \xi_R(t_n), \end{aligned} \quad (9)$$

$$\begin{aligned}
\mathbf{r}(t_n) = & \mathbf{r}(t_{n-1}) + v \left[\hat{\mathbf{N}}(t_n) - \hat{\mathbf{N}}(t_{n-1}) \right] \\
& + \sum_{j=1}^{n-1} c_{n-j} \left\{ v \left[\hat{\mathbf{N}}(t_j) - \hat{\mathbf{N}}(t_{j-1}) \right] - (\mathbf{r}(t_j) - \mathbf{r}(t_{j-1})) \right\} \\
& + \frac{\Gamma(2 - \alpha_T)}{h^{-\alpha_T}} \theta_T \xi_T(t_n),
\end{aligned} \tag{10}$$

where $c_k = (k+1)^{1-\alpha_Q} - k^{1-\alpha_Q}$, $\hat{\mathbf{N}}(t_j) - \hat{\mathbf{N}}(t_{j-1}) \approx h[\cos \phi(t_j), \sin \phi(t_j)]$, and the algorithm achieves a local precision of $O(h^{2-\alpha_Q})$ [49, 50].

We calculated numerical solutions for the angular and translational components $(\phi(t_n), x(t_n), y(t_n))$ using Eqs. (9) and (10) with uniformly distributed initial angle $\phi_0 \sim U[0, \pi]$ and $x_0 = y_0 = 0$. The rotational and translational noises were generated from fractional Brownian motion trajectories using the Python library fBm0.3.0 [51], and then differentiated to obtain the fractional Gaussian noises $\theta_R \xi_R(t_n) = [B_{H_R}(t_n) - B_{H_R}(t_{n-1})]h^{-1}$ and $\theta_T \xi_T(t_n) = [B_{H_T}(t_n) - B_{H_T}(t_{n-1})]h^{-1}$. Numerical MSDs were calculated directly as $(\phi(t_n) - \phi_0)^2$ and $(\mathbf{r}(t_n) - \mathbf{r}_0)^2$, averaged over 3000 independent trajectories. We defined the characteristic timescale of the rotational component as $\tau_R = [\Gamma(1 + \alpha_R)D_R/2]^{-1/\alpha_R} = [\eta_R/k_B T]^{1/\alpha_R}$, where $D_R = 2k_B T/[\eta_R \Gamma(1 + \alpha_R)]$ is the rotational diffusion coefficient. For all the numerics, we computed 95% normal confidence intervals.

In Fig. 1(a), we present the numerical calculation of the angular MSD and compare it with the analytical result $\langle(\phi(t) - \phi_0)^2\rangle = D_R t^{\alpha_R}$ derived in the App. B of the End Matter. Analytical expressions are shown as brown solid lines, while colored markers represent sampled points from the numerical solutions, and the shaded areas indicate the 95% confidence intervals. The same scaling holds for the passive translational motion ($v = 0$), with an additional factor of 2 accounting for the contributions of both x and y . The thermalization behavior of the numerical algorithm is analyzed in the inset of Fig. 1(a) for fixed $h = 0.005$ and $\alpha_R = \{0.2, 0.7\}$. For $\alpha_R = 0.2$ (orange), the convergence to the overdamped limit occurs on a time scale $\mathcal{O}[10t/\tau_R]$, whereas for $\alpha_R = 0.7$ (yellow), the convergence is much faster, $\mathcal{O}[10^{-1}t/\tau_R]$. To improve accuracy and speed-up thermalization, we therefore set the time step at $h = 5 \times 10^{-5}$ for $\alpha_R = 0.2$, $h = 0.001$ for $\alpha_R = 0.3$, and kept $h = 0.005$ for $\alpha_R > 0.3$, in all subsequent numerical calculations.

Autocorrelation of the self-propulsion direction—A common assumption for GLEs driven by Gaussian noise is that their solutions are linear combinations of Gaussian processes, so the process itself is asymptotically Gaussian [52, 53]. Although the rigorous construction of the corresponding Fokker–Planck equation for a non-Markovian process remains an open problem [54–57], and is generally non-Gaussian (except in the case of fractional Brownian motion [54]), this Gaussian approximation allows us to simplify the analytical calculations and to systematically study the statistical properties of the self-propulsion di-

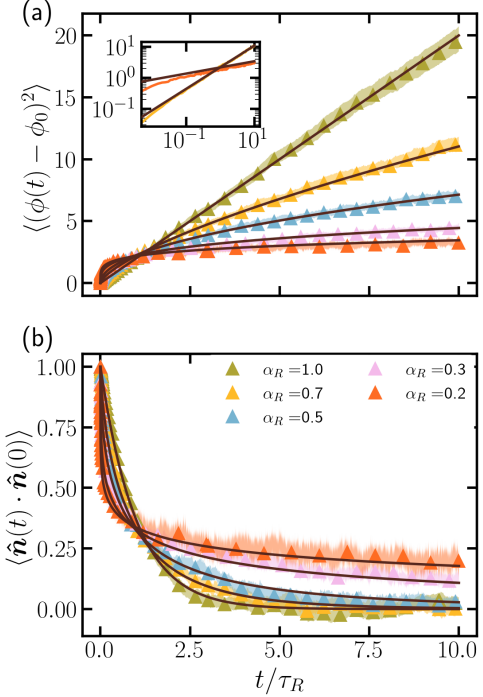


FIG. 1. Dynamics of the angular component of an active Brownian particle for different fractional orders α_R . Analytical expressions are shown as solid brown lines, while colored markers represent sampled points from numerical simulations with 95% confidence bands. (a) Angular MSD in units of rad^2 . The inset illustrates the thermalization of the numerical solutions toward the overdamped limit for $\alpha_R = 0.2$ (orange) and $\alpha_R = 0.7$ (yellow), using a time step $h = 0.005$. (b) Autocorrelation function of the self-propulsion direction. All curves are normalized by the rotational timescale $\tau_R = (\eta_R/k_B T)^{1/\alpha_R}$.

rection. Hence, we assume that the angular displacement follows a Gaussian distribution with zero-mean $\mu_\phi = 0$ and variance $\sigma_\phi^2 = \langle(\phi - \phi_0)^2\rangle + |\phi_0|^2$. The autocorrelation of the self-propulsion direction then reads

$$\langle \hat{\mathbf{n}}(t) \cdot \hat{\mathbf{n}}(t') \rangle = \langle \cos[\Delta\phi(t)] \rangle = e^{-\frac{D_R|t-t'|^{\alpha_R}}{2}}, \tag{11}$$

which stems from the standard result for the cosine of a Gaussian variable X with mean μ_X and variance σ_X^2 , $\langle \cos(X) \rangle = \Re\langle \exp(iX) \rangle = \cos(\mu_X) \exp(-\sigma_X^2/2)$ [46, 58].

In Fig. 1(b), we present numerical results for the autocorrelation of the self-propulsion direction and compare them with Eq. (11) for $t' = 0$ and various values of α_R . The area under the autocorrelation curves corresponds to the persistence time, which is the average time the particle maintains its orientation. Using the change of variables $s = D_R t^{\alpha_R}/2$, it can be calculated by integrating Eq. (11), $\tau_p = \int_0^\infty \langle \hat{\mathbf{n}}(t) \cdot \hat{\mathbf{n}}(0) \rangle dt = (2/D_R)^{1/\alpha_R} \Gamma(1 + 1/\alpha_R)$. For $\alpha_R = 1$, it retrieves the standard persistence time for conventional active Brownian particles $\tau_p = 2/D_R$, where the orientation decays exponentially. For $\alpha_R < 1$, however, memory effects induced by the fractional operator stretch the decorre-

lation time. Consequently, decreasing α_R increases the persistence of the orientation, which diverges in the limit $\lim_{\alpha_R \rightarrow 0} \tau_P \rightarrow \infty$. Furthermore, we observed two distinct trends: for $\alpha_R \geq 0.5$, the persistence time decays rapidly toward the lower limit $\alpha_R = 1$, while for $\alpha_R < 0.5$, the decorrelation time is strongly stretched.

In Ref. [59], active Brownian particles were modeled with a rotational component described by linear friction and driven by fractional Brownian motion. In that case, the persistence time depends on the Hurst exponent $0 < H_R < 1$ as $(2/D_H)^{1/2H_R}$, where D_H is a Hurst-

dependent rotational diffusion coefficient. Smaller values of H_R increase the persistence time and reinforce long-range correlations, while $H_R = 1/2$ reduces to the conventional active Brownian particle behavior. In contrast, the order of the fractional derivative and the rotational Hurst exponent in Eqs.(1) are coupled via $\alpha_R = 2 - 2H_R$, with $1/2 \leq H_R < 1$, as imposed by the fluctuation-dissipation theorem. This coupling implies that higher H_R values strengthen long-range correlations and extends the persistence time, since our model is defined only within the persistent regime of fractional Brownian motion.

Active diffusion—The total MSD of an active particle can be calculated from the solutions given by Eq. (7). Using the results derived in App. B and App. C of the End Matter, we obtain

$$\begin{aligned} \langle(\mathbf{r} - \mathbf{r}_0)^2\rangle &= \int_0^t d\tau_1 G_T(\tau_1) \int_0^t d\tau_2 G_T(\tau_2) \text{Tr}[\mathbb{C}_T(|\tau_1 - \tau_2|)] + v^2 \int_0^t d\tau_1 \int_0^t d\tau_2 \langle \hat{\mathbf{n}}(\tau_1) \cdot \hat{\mathbf{n}}(\tau_2) \rangle \\ &= 2D_T t^{\alpha_T} + \frac{2v^2}{\alpha_R (D_R/2)^{\frac{2}{\alpha_R}}} \left[\gamma\left(\frac{1}{\alpha_R}, \frac{D_R}{2} t^{\alpha_R}\right) \left(\frac{D_R}{2}\right)^{\frac{1}{\alpha_R}} t - \gamma\left(\frac{2}{\alpha_R}, \frac{D_R}{2} t^{\alpha_R}\right) \right], \end{aligned} \quad (12)$$

where D_T denotes the translational diffusion coefficient and $\gamma(a, z)$ is the lower incomplete Gamma function.

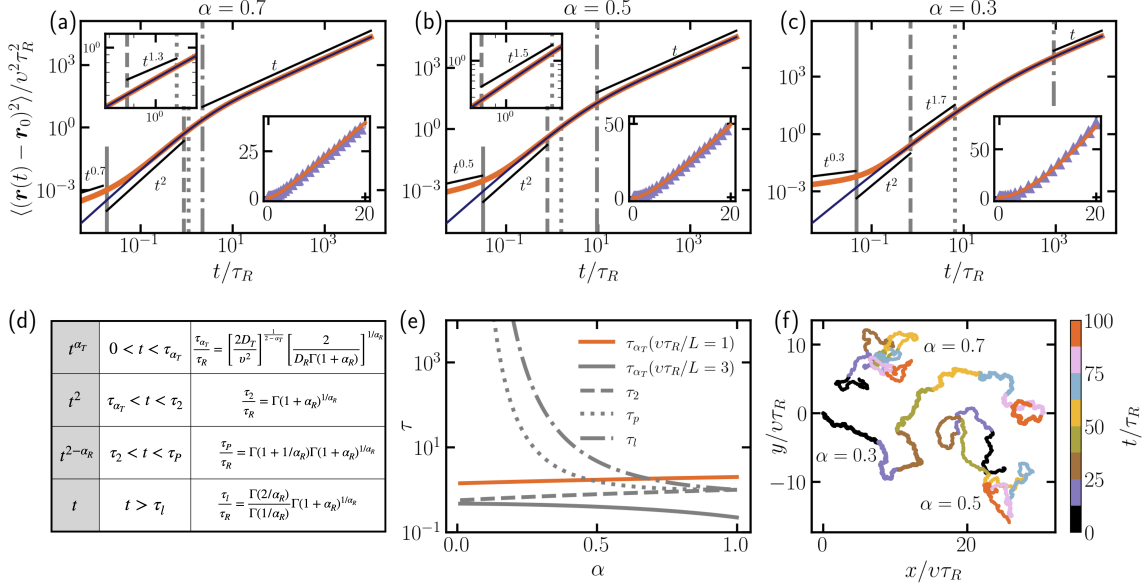


FIG. 2. Active diffusion regimes for $\alpha \equiv \alpha_R = \alpha_T$. (a)-(c) MSD for $v\tau_R/L = 20$ (solid orange line) and $v\tau_R/L = \infty$ (solid navy) for $\alpha = 0.7, 0.5, 0.3$, respectively. Bottom-right insets show the comparison between analytical and numerical results, while top-left insets present a zoom into the $t^{2-\alpha_R}$ superdiffusive regime. Crossover times between diffusion regimes are indicated by grey lines using the convention: τ_{α_T} -solid, τ_2 -dashed, τ_p -dotted and τ_l -dotted-dashed. (d) Summary of the diffusion regimes. (e) Crossover times as a function of α . (f) Representative particle trajectories for each α . All times-scales are in units of τ_R , and all spatial coordinates are normalized by the characteristic length $v\tau_R$.

When $\alpha_R = \alpha_T = 1$, Eq. (12) recovers the conventional result for active Brownian particles, where the MSD exhibits an initial short-time diffusive regime, followed by an active persistent scaling behavior t^2 , and fi-

nally a crossover to long-time normal diffusion t with an enhanced diffusion coefficient [60]. Additionally, Eq. (12) reproduces the results of Ref. [59] when imposing $\alpha_R = 2H_R$, corresponding to a fractional rotational noise with

linear dissipation. However, when the fractional orders differ from one and satisfy the thermal condition $\alpha_Q = 2 - 2H_Q$, a rich variety of dynamical regimes emerges. At short times, a competition between translational subdiffusion and the active persistent phase occurs, with a crossover time $\tau_{\alpha_T} = (2D_T/v^2)^{1/(2-\alpha_T)}$ marking the transition from t^{α_T} to t^2 . Within the persistent phase, the MSD exhibits a second transition from ballistic t^2 to sub-ballistic superdiffusive $t^{2-\alpha_R}$. From the series expansion of the active MSD (see App. C of the End Matter), the characteristic crossover time is $\tau_2 = (2/D_R)^{1/\alpha_R}$, since for small times $D_R t^{\alpha_R}/2 \ll 1$, the leading contribution is vt^2 . At long times, the system relaxes to normal diffusion with the long-time diffusion coefficient, $D_l = 2\nu^2\Gamma(1+1/\alpha_R)/(D_R/2)^{1/\alpha_R}$, and the corresponding linear regime is reached for $t > \tau_l$, where $\tau_l = (2/D_R)^{1/\alpha_R}\Gamma(2/\alpha_R)/\Gamma(1/\alpha_R)$ is the characteristic timescale at which the first incomplete gamma function dominates over the second one in Eq.(12).

In Fig. 2, we illustrate the diffusion regimes for fixed $\alpha \equiv \alpha_R = \alpha_T$, with values $\alpha = \{0.7, 0.5, 0.3\}$. Panels (a)-(c) present the analytical MSD from Eq. (12), with $v\tau_R/L = 20$ in orange solid lines and $v\tau_R/L = \infty$ in solid navy, where L denotes a unit length. The crossover times between regimes are represented by grey lines following the convention: τ_{α_T} -solid, τ_2 -dashed, τ_p -dotted and τ_l -dotted-dashed. The case $v\tau_R/L = \infty$ is effectively reached when $v^2 \gg 2D_T$, where the short-time behavior is fully dominated by the t^2 active persistent phase, and the initial translational subdiffusion is negligible. In contrast, $v\tau_R/L = 20$ still allows for a brief subdiffusive regime at very early times. The comparison between analytical and numerical results is shown in the bottom-right insets, while the top-left insets provide a zoom into the $t^{2-\alpha_R}$ super-diffusive regime. The sequence of MSD regimes is summarized in Fig. 2(d).

When $\alpha > 0.5$, the timescales τ_2, τ_p, τ_l approach each other and collapse at the Newtonian limit $\alpha = 1$. Furthermore, for small $v\tau_R/L$, the timescale τ_{α_T} partially dominates over τ_p and τ_l for $\alpha \geq 0.5$ and fully suppresses the t^2 dynamics across the entire α range, as demonstrated by the orange line in Fig. 2(e). For $\alpha < 0.5$, both the superdiffusive regime and the approach to normal diffusion are over-stretched, diverging in the limit $\alpha \rightarrow 0$, and favoring superdiffusion over ballistic behavior. Using Stirling's approximation for the Gamma function $\Gamma(z) = \sqrt{2\pi/z(z/e)^z}[1 + \mathcal{O}(1/z)]$, we analyze the divergent behavior of the characteristic timescales. For $z = 1 + 1/\alpha$ with $1/\alpha \gg 1$, the persistence time is approximately $\tau_p/\tau_R = \Gamma(1 + 1/\alpha)\Gamma(1 + \alpha)^{1/\alpha} \approx \sqrt{2\pi/\alpha}(1/\alpha e)^{1/\alpha}$, τ_R normalizes the timescale to remove the dependence on D_R , and $\Gamma(1 + \alpha)^{1/\alpha} \approx 1$. Similarly, the long-time diffusion scale is $\tau_l/\tau_R = \Gamma(2/\alpha)\Gamma(1 + \alpha)^{1/\alpha}/\Gamma(1/\alpha) \approx \sqrt{2}(4/\alpha e)^{1/\alpha}$, so that $\tau_l/\tau_p \approx \sqrt{\alpha/\pi}4^{1/\alpha}$. This shows that the effective diffusion time τ_l grows exponentially faster than the persistence time τ_p in the limit $1/\alpha \gg 1$. The dependence of the timescales on α is shown in Fig. 2(e), while Fig. 2(f) shows sample trajectories for

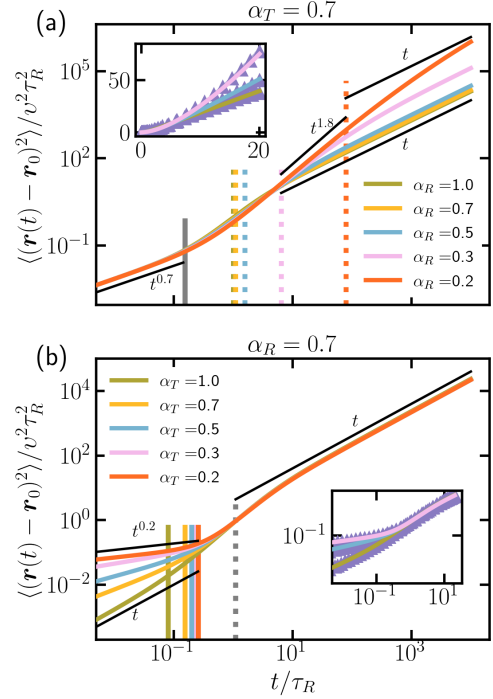


FIG. 3. Diffusion regimes for decoupled translational and rotational orders. Analytical MSDs are presented in solid colored lines while numerical results are shown in purple in the figure insets. The relevant timescales τ_{α_T} and τ_p are represented, respectively, in vertical solid and dotted lines, following the color convention of the MSD. (a) MSD for fixed $\alpha_T = 0.7$. (b) MSD for $\alpha_R = 0.7$. Times are normalized by τ_R and spatial variables by the characteristic length $v\tau_R$.

each α . A marked difference is observed for $\alpha = 0.3$, where the over-stretching of τ_p causes superdiffusive motion extending up to $t/\tau_R \approx 100$.

Finally, we analyze the effect of decoupling α_R and α_T . In Fig. 3, we illustrate this by fixing either $\alpha_T = 0.7$ or $\alpha_R = 0.7$. The analysis of time scales presented above holds when $\alpha_R \neq \alpha_T$, as there is no cross-dependence between time scales and fractional orders. When α_T is fixed and α_R is varied [Fig. 3(a)], the short-time dynamics is dominated by t^{α_T} up to the crossover time τ_{α_T} , while the persistent regime exhibits an initial t^2 ballistic behavior, followed by a super-diffusive spectrum between t and t^2 , and finally relaxes to linear diffusion at times determined by the dependence of τ_l on α_R . On the other hand, varying α_T only affects the short-time dynamics, see Fig. 3(b). As α_T decreases, the persistent phase becomes shorter due to the enhanced memory effects associated with the dominant elastic properties of the medium, while the long-time diffusion remains governed by the fixed α_R .

Conclusion—Our results provide new insights into the dynamics of active particles in power-law viscoelastic materials, a class of media that is highly relevant in soft and biological matter. We uncovered a rich variety of diffu-

sive, subdiffusive, and superdiffusive regimes and identified the corresponding characteristic length and time scales, revealing a competition between translational and rotational contributions. This competition results in a persistent regime that favors an over-stretched superdiffusive motion over a ballistic one, effectively questioning the relation between persistence and propulsion in active

matter. The analytical and numerical framework developed here can be extended to investigate more complex active behaviors, such as collective phases or optimized motion strategies. Moreover, we anticipate that our findings will contribute to the understanding of experimental observations of active particles in diverse media ranging from gels [23–25], polymer networks [30–32] and crowded environments [17, 33, 34].

-
- [1] M. te Vrugt, B. Liebchen, and M. E. Cates, What exactly is ‘active matter’? (2025), arXiv:2507.21621.
- [2] C. Bechinger, R. Di Leonardo, H. Löwen, C. Reichhardt, G. Volpe, and G. Volpe, Active particles in complex and crowded environments, *Rev. Mod. Phys.* **88**, 045006 (2016).
- [3] S. Ramaswamy, The mechanics and statistics of active matter, *Annu. Rev. Condens. Matter Phys.* **1**, 323 (2010).
- [4] T. Vicsek, A. Czirók, E. Ben-Jacob, I. Cohen, and O. Shochet, Novel type of phase transition in a system of self-driven particles, *Phys. Rev. Lett.* **75**, 1226 (1995).
- [5] H. Chaté, F. Ginelli, G. Grégoire, F. Peruani, and F. Raynaud, Modeling collective motion: variations on the vicsek model, *Eur. Phys. J. B* **64**, 451 (2008).
- [6] Z. Liu and M. Dijkstra, Collective dynamics of intelligent active Brownian particles with visual perception and velocity alignment in 3d: spheres, rods, and worms, *Soft Matter* **21**, 1529 (2025).
- [7] Z. Budrikis, Collective motion strategies of sheep, *Nat. Rev. Phys.* **5**, 82 (2023).
- [8] L. Turner, R. Zhang, N. C. Darnton, and H. C. Berg, Visualization of flagella during bacterial swarming, *J. Bacteriol.* **192**, 3259 (2010).
- [9] J. Elgeti, R. G. Winkler, and G. Gompper, Physics of microswimmers—single particle motion and collective behavior: a review, *Rep. Prog. Phys.* **78**, 056601 (2015).
- [10] S. Thakur and R. Kapral, Dynamics of self-propelled nanomotors in chemically active media, *J. Chem. Phys.* **135**, 024509 (2011).
- [11] H. Löwen, Gigantic dynamical spreading and anomalous diffusion of jerky active particles (2025), arXiv:2507.08910.
- [12] W. Zhong, Anomalous collective diffusion in two-dimensional active particle systems, *Phys. Rev. E* **112**, 054112 (2025).
- [13] J. Stenhammar, D. Marenduzzo, R. J. Allen, and M. E. Cates, Phase behaviour of active Brownian particles: the role of dimensionality, *Soft Matter* **10**, 1489 (2014).
- [14] T. Surrey, F. Nédélec, S. Leibler, and E. Karsenti, Physical properties determining self-organization of motors and microtubules, *Science* **292**, 1167 (2001).
- [15] R. Lakes, *Viscoelastic Materials* (Cambridge Univ. Press, Cambridge, 2009).
- [16] T. G. Mason, Estimating the viscoelastic moduli of complex fluids using the generalized Stokes–Einstein equation, *Rheol. Acta* **39**, 371 (2000).
- [17] T. G. Mason, H. Gang, and D. A. Weitz, Diffusing-wave-spectroscopy measurements of viscoelasticity of complex fluids, *J. Opt. Soc. Am. A* **14**, 139 (1997).
- [18] N. Narinder, C. Bechinger, and J. R. Gomez-Solano, Memory-induced transition from a persistent random walk to circular motion for achiral microswimmers, *Phys. Rev. Lett.* **121**, 078003 (2018).
- [19] A. R. Sprenger, C. Bair, and H. Löwen, Active Brownian motion with memory delay induced by a viscoelastic medium, *Phys. Rev. E* **105**, 044610 (2022).
- [20] A. Bonfanti, J. L. Kaplan, G. Charras, and A. Kabla, Fractional viscoelastic models for power-law materials, *Soft Matter* **16**, 6002 (2020).
- [21] T. G. Mason and D. A. Weitz, Optical measurements of frequency-dependent linear viscoelastic moduli of complex fluids, *Phys. Rev. Lett.* **74**, 1250 (1995).
- [22] R. Sinkus, K. Siegmann, T. Xydeas, M. Tanter, C. Claussen, and M. Fink, MR elastography of breast lesions: Understanding the solid/liquid duality can improve the specificity of contrast-enhanced mr mammography, *Magn. Reson. Med.* **58**, 1135 (2007).
- [23] S. Aney, P. Pandit, L. Ratke, and et al., On the origin of power-scaling exponents in silica aerogels, *J. Sol-Gel Sci. Technol.* **114**, 98 (2025).
- [24] S. Aime, L. Cipelletti, and L. Ramos, Power law viscoelasticity of a fractal colloidal gel, *J. Rheol.* **62**, 1429 (2018).
- [25] T. S. K. Ng and G. H. McKinley, Power law gels at finite strains: The nonlinear rheology of gluten gels, *J. Rheol.* **52**, 417 (2008).
- [26] F. Gittes, B. Schnurr, P. D. Olmsted, F. C. MacKintosh, and C. F. Schmidt, Microscopic viscoelasticity: Shear moduli of soft materials determined from thermal fluctuations, *Phys. Rev. Lett.* **79**, 3286 (1997).
- [27] M. Dichtl and E. Sackmann, Colloidal probe study of short time local and long time reptational motion of semi-flexible macromolecules in entangled networks, *New J. Phys.* **1**, 18 (1999).
- [28] A. Caspi, R. Granek, and M. Elbaum, Enhanced diffusion in active intracellular transport, *Phys. Rev. Lett.* **85**, 5655 (2000).
- [29] E. Flenner, J. Das, M. C. Rheinstädter, and I. Kosztin, Subdiffusion and lateral diffusion coefficient of lipid atoms and molecules in phospholipid bilayers, *Phys. Rev. E* **79**, 011907 (2009).
- [30] S. Joo, X. Durang, O.-c. Lee, and J.-H. Jeon, Anomalous diffusion of active Brownian particles cross-linked to a polymer network, *Soft Matter* **16**, 9188 (2020).
- [31] S. Mani, H. H. Winter, M. Silverstein, and et al., Power law relaxation in an interpenetrating polymer network, *Colloid Polym. Sci.* **267**, 1002 (1989).
- [32] Z. Zhang, E. Bouchbinder, and E. Lerner, The strain-stiffening critical exponents in polymer networks and their universality, *J. Chem. Phys.* **163**, 111102 (2025).
- [33] A. Maiti, Y. Koyano, H. Kitahata, and K. K. Dey, Activity-induced diffusion recovery in crowded colloidal

- suspensions, Phys. Rev. E **109**, 054607 (2024).
- [34] H. Ebata and K. e. a. Nishizawa, Single power-law rheology of crowded cytoplasm in living cells (2025), arXiv:2504.18922.
- [35] S. Joo and J.-H. Jeon, Viscoelastic active diffusion governed by nonequilibrium fractional Langevin equations: Underdamped dynamics and ergodicity breaking, Chaos, Solitons Fractals **177**, 114288 (2023).
- [36] Y. Kang, S. Seo, S. Kwon, and K. Kim, Fractional motion of an active particle in fractional generalized Langevin equations, Fractal Fract. **9**, 725 (2025).
- [37] R. Metzler and T. F. Nonnenmacher, Fractional relaxation processes and fractional rheological models, Int. J. Plast. **19**, 941 (2003).
- [38] R. Hilfer, *Applications of Fractional Calculus in Physics* (World Scientific, Singapore, 2000).
- [39] D. Klatt, U. Hamhaber, P. Asbach, J. Braun, and I. Sack, Noninvasive assessment of the rheological behavior of human organs using multifrequency mr elastography: a study of brain and liver viscoelasticity, Phys. Med. Biol. **52**, 7281 (2007).
- [40] F. C. Meral, T. J. Royston, and R. Magin, Fractional calculus in viscoelasticity: An experimental study, Commun. Nonlinear Sci. Numer. Simul. **15**, 939 (2010).
- [41] R. Metzler and J. Klafter, The random walk's guide to anomalous diffusion: a fractional dynamics approach, Phys. Rep. **339**, 1 (2000).
- [42] E. Lutz, Fractional Langevin equation, Phys. Rev. E **64**, 051106 (2001).
- [43] D. S. Quevedo, R. C. Verstraten, and C. Morais Smith, Emergent transient time crystal from a fractional Langevin equation with white and colored noise, Phys. Rev. A **110**, 052208 (2024).
- [44] R. C. Verstraten, R. F. Ozela, and C. M. Smith, Time glass: A fractional calculus approach, Phys. Rev. B **103**, L180301 (2021).
- [45] M. Caputo, Linear models of dissipation whose Q is almost frequency independent—II, Geophys. J. Int **13**, 529 (1967).
- [46] H. Risken, *The Fokker-Planck equation: methods of solution and applications*, Vol. 2 (Springer. Heidelberg, Germany., 1989).
- [47] S. F. Kwok, *Langevin and Fokker-Planck Equations and Their Generalizations: Descriptions and Solutions* (World Scientific. New Jersey, USA, 2018).
- [48] P. Guo, C. Zeng, C. Li, and Y. Chen, Numerics for the fractional Langevin equation driven by the fractional Brownian motion, Fract. Calc. Appl. Anal. **16**, 123 (2013).
- [49] M. Murillo-Arcila, A. Peris, and Á. Vargas-Moreno, Dynamics of the caputo fractional derivative, Fract. Calc. Appl. Anal. **1** (2025).
- [50] C. Li and F. Zeng, *Numerical methods for fractional calculus*, Vol. 24 (CRC Press, 2015).
- [51] C. Flynn, fbm 0.3.0: Fractional Brownian motion realizations. (2019).
- [52] K. Wang, Long-time-correlation effects and biased anomalous diffusion, Phys. Rev. A **45**, 833 (1992).
- [53] J. M. Porra, K.-G. Wang, and J. Masoliver, Generalized Langevin equations: Anomalous diffusion and probability distributions, Phys. Rev. E **53**, 5872 (1996).
- [54] I. Calvo and R. Sanchez, The path integral formulation of fractional Brownian motion for the general Hurst exponent, J. Phys. A: Math. Theor. **41**, 282002 (2008).
- [55] P. Hänggi, Correlation functions and masterequations of generalized (non-markovian) langevin equations, Z. Phys. B: Condens. Matter **31**, 407 (1978).
- [56] S. Khan and A. M. Reynolds, Derivation of a Fokker-Planck equation for generalized Langevin dynamics, Physica A **350**, 183 (2005).
- [57] D. S. Quevedo, F. S. Abril-Bermúdez, and C. Morais Smith, Path integral and generalized Klein-Kramers equation for Langevin dynamics with fractional Gaussian noise, arXiv preprint (2026).
- [58] P. K. Ghosh, Y. Li, G. Marchegiani, and F. Marchesoni, Communication: Memory effects and active Brownian diffusion, J. Chem. Phys. **143** (2015).
- [59] J. R. Gomez-Solano and F. J. Sevilla, Active particles with fractional rotational Brownian motion, Jour. Stat. Mech: Theory Exp. **2020**, 063213 (2020).
- [60] G. Volpe, S. Gigan, and G. Volpe, Simulation of the active Brownian motion of a microswimmer, Am. J. Phys. **82**, 659 (2014).
- [61] F. Mainardi and R. Gorenflo, On Mittag-Leffler-type functions in fractional evolution processes, J. Comput. Appl. Math. **118**, 283 (2000).

End Matter

Appendix A. L1 discretization of the fractional active Langevin equations—On a uniform time grid $t_j = k * h$ with h the step size and $k \in [0, \dots, n]$, the integral over the time interval in Eq. (3) can be split into the sum of n contributions,

$${}_0^C D_t^{\alpha_Q} q = \frac{1}{\Gamma(1 - \alpha_Q)} \sum_{j=1}^n \int_{t_{j-1}}^{t_j} (t_n - \tau)^{-\alpha_Q} q'(\tau) d\tau.$$

The first-order derivative of q can be approximated using a finite difference scheme $hq'(\tau) \approx q(t_j) - q(t_{j-1})$, leading

to

$$\int_{t_{j-1}}^{t_j} (t - \tau)^{-\alpha_Q} \frac{dq}{d\tau} d\tau \approx \frac{q(t_j) - q(t_{j-1})}{h} \int_{t_{j-1}}^{t_j} (t_n - \tau)^{-\alpha_Q} d\tau.$$

The kernel integral can be exactly evaluated to

$$\int_{t_{j-1}}^{t_j} (t - \tau)^{-\alpha_Q} d\tau = \frac{(t_n - t_{j-1})^{1-\alpha_Q} - (t_n - t_j)^{1-\alpha_Q}}{(1 - \alpha_Q)},$$

where $t_n - t_{j-1} = (n - j + 1)h$ and $t_n - t_j = (n - j)h$. Factoring out the time step h , we get the L1 Caputo discretization

$${}_{t_0}^C D_t^{\alpha_Q} q = \frac{h^{-\alpha_Q}}{\Gamma(2 - \alpha_Q)} \sum_{j=1}^n c_{n-j} [q(t_j) - q(t_{j-1})], \quad (\text{A1})$$

with $c_k = (k + 1)^{1 - \alpha_Q} - k^{1 - \alpha_Q}$.

Applying Eq. (A1) to the rotational and translational components of the fractional active Langevin equation,

we obtain the recursive relations in Eqs. (9) and (10). In particular, the increments of the self-propulsion direction can be further simplified by assuming a right-endpoint approximation,

$$\begin{aligned} \hat{\mathbf{N}}(t_j) - \hat{\mathbf{N}}(t_{j-1}) &= \int_{t_{j-1}}^{t_j} [\cos \phi(t), \sin \phi(t)] dt \\ &\approx h[\cos \phi(t_j), \sin \phi(t_j)]. \end{aligned} \quad (\text{A2})$$

Appendix B. Passive under- and over-damped dynamics—When $v\tau_R/L = 0$, the set of fractional Eqs. (4) has the same form for both spatial and angular degrees of freedom. In this case, we can generically write the overdamped fractional Langevin equation,

$$\eta_Q {}_0^C D_t^{\alpha_Q} q(t) = \theta_Q \xi_q(t), \quad (\text{B1})$$

with $q = \{x, y, \phi\}$ representing a general coordinate for space and angle, and $\xi_q = \{\xi_x, \xi_y, \xi_R\}$ the corresponding noise satisfying Eq. (5). The general solution to Eq.(B1) is given by $q(t) = q_0 + \theta_Q (\xi_q * G_Q)(t)$. Therefore, the passive MSD is

$$\begin{aligned} \langle (q - q_0)^2 \rangle &= \int_0^t d\tau_1 G_Q(\tau_1) \int_0^t d\tau_2 G_Q(\tau_2) C_q(|\tau_1 - \tau_2|) \\ &= 2 \int_0^t d\tau_1 G_Q(\tau_1) \int_0^{\tau_1} d\tau_2 G_Q(\tau_2) C_q(\tau_1 - \tau_2) \\ &= \frac{2\theta_q^2 H_Q(2H_Q - 1)}{\eta_Q^2 \Gamma^2(\alpha_Q)} \int_0^t d\tau_1 \tau_1^{\alpha_Q - 1} \int_0^{\tau_1} d\tau_2 \tau_2^{\alpha_Q - 1} (\tau_1 - \tau_2)^{-\alpha_Q}, \end{aligned} \quad (\text{B2})$$

where the second line relies on splitting the squared integration domain into two equal triangular areas at $\tau_1 = \tau_2$ and exchanging the variables $\tau_1 \leftrightarrow \tau_2$. The second integral can be simplified by converting it into an Euler Beta function $\mathbf{B}(a, b) = \int_0^1 z^{a-1} (1-z)^{b-1}$, using the change of variables $\tau_2 = \tau_1 z$ together with the properties $\mathbf{B}(a, b) = \Gamma(a)\Gamma(b)/\Gamma(a+b)$ and $z\Gamma(z) = \Gamma(z+1)$,

$$\begin{aligned} \langle (q - q_0)^2 \rangle &= \frac{2\theta_q^2 H_Q(2H_Q - 1)}{\eta_Q^2 \Gamma^2(\alpha_Q)} \int_0^t d\tau_1 \tau_1^{\alpha_Q - 1} \int_0^1 dz z^{\alpha_Q - 1} (1-z)^{-\alpha_Q} \\ &= \frac{2\theta_q^2 H_Q(2H_Q - 1) \mathbf{B}(\alpha_Q, 1 - \alpha_Q)}{\eta_Q^2 \Gamma^2(\alpha_Q)} \int_0^t d\tau_1 \tau_1^{\alpha_Q - 1} \\ &= \frac{2\theta_q^2 H_Q(2H_Q - 1) \Gamma(1 - \alpha_Q)}{\eta_Q^2 \Gamma(\alpha_Q + 1)} t^{\alpha_Q} \\ &= D_Q t^{\alpha_Q}, \end{aligned} \quad (\text{B3})$$

where we replaced $\theta_Q^2 = \eta_T k_B T / [\Gamma(1 - \alpha_Q) H_R (2H_R - 1)]$ and defined the diffusion coefficient $D_Q = 2k_B T / [\eta_Q \Gamma(1 + \alpha_Q)]$.

The underdamped counterpart of Eq. (B1) is the so-called fractional Langevin equation [42],

$$m\ddot{q}(t) + \eta_Q {}_0^C D_t^{\alpha_Q} q(t) = \theta_Q \xi_q(t). \quad (\text{B4})$$

The resolvent function of this equation is the more general result written in terms of the Mittag-Leffler function $E_{a,b}(z) = \sum_{k=0}^{\infty} z^k / \Gamma(ak + b)$ [61],

$$G_u = t E_{2-\alpha_Q, 2} \left(\frac{\eta_Q}{m} t^{2-\alpha_Q} \right),$$

where the typical relaxation timescale is $\tau_u = (m/\eta_Q)^{1/2-\alpha_Q}$. In the long-term limit, $t \gg \tau_u$, the inertial effects from the mass m can be neglected, and the resolvent reduces to our result in Eq. (8), $G_Q = \lim_{t \rightarrow \infty} G_u / m$. Furthermore, the MSD (B3) also coincides with the long-term anomalous diffusion limit of the underdamped equation. Thus,

Eq. (B1) describes the overdamped dynamics of the system by assuming that at $t = 0$ the stationary state has already been reached.

Appendix C. Derivation of the active rotational MSD—Replacing the autocorrelation of the self-propulsion direction, given by Eq. (11), in the expression for the total MSD (12) and changing the integration domain as in Eq. (B3), we obtain

$$\begin{aligned} \langle(\mathbf{r} - \mathbf{r}_0)^2\rangle_a &= v^2 \int_0^t d\tau_1 \int_0^t d\tau_2 \langle \hat{\mathbf{n}}(\tau_1) \cdot \hat{\mathbf{n}}(\tau_2) \rangle \\ &= v^2 \int_0^t d\tau_1 \int_0^t d\tau_2 e^{-\frac{D_R}{2}|\tau_1 - \tau_2|^{\alpha_R}} \\ &= 2v^2 \int_0^t d\tau_1 \int_0^{\tau_1} d\tau_2 e^{-\frac{D_R}{2}(\tau_1 - \tau_2)^{\alpha_R}} \\ &= 2v^2 \int_0^t d\tau_1 \int_0^{\tau_1} d\tau e^{-\frac{D_R}{2}\tau^{\alpha_R}}, \end{aligned} \quad (\text{C1})$$

where we made the change of variables $\tau = \tau_1 - \tau_2$.

Now, using the power-series representation of the exponential and integrating, we obtain

$$\begin{aligned} \langle(\mathbf{r} - \mathbf{r}_0)^2\rangle_a &= 2v^2 \int_0^t d\tau_1 \int_0^{\tau_1} d\tau \sum_{k=0}^{\infty} \frac{(-\frac{D_R}{2}\tau^{\alpha_R})^k}{k!} \\ &= 2v^2 t^2 \sum_{k=0}^{\infty} \frac{(-\frac{D_R}{2}t^{\alpha_R})^k}{k!(k\alpha_R + 1)(k\alpha_R + 2)} \\ &= \frac{2v^2 t^2}{\alpha_R} \left[\sum_{k=0}^{\infty} \frac{(-\frac{D_R}{2}t^{\alpha_R})^k}{k!(k + 1/\alpha_R)} - \sum_{k=0}^{\infty} \frac{(-\frac{D_R}{2}t^{\alpha_R})^k}{k!(k + 2/\alpha_R)} \right]. \end{aligned} \quad (\text{C2})$$

The last line in Eq. (C2) can be simplified using the power-series representation of the lower incomplete Gamma function,

$$\gamma(z, a) = \int_0^a t^{z-1} e^{-t} dt = a^z \sum_{k=0}^{\infty} \frac{(-a)^k}{k!(k+z)}, \quad (\text{C3})$$

to obtain

$$\langle(\mathbf{r} - \mathbf{r}_0)^2\rangle_a = \frac{2v^2}{\alpha_R (D_R/2)^{\frac{2}{\alpha_R}}} \left[\gamma\left(\frac{1}{\alpha_R}, \frac{D_R}{2}t^{\alpha_R}\right) \left(\frac{D_R}{2}\right)^{\frac{1}{\alpha_R}} t - \gamma\left(\frac{2}{\alpha_R}, \frac{D_R}{2}t^{\alpha_R}\right) \right]. \quad (\text{C4})$$